

The Simulation of 3D Flows in Blade Rows and Exhaust Systems using a Multiblock Navier-Stokes Solver

Jian-Jun LIU

Institute of Engineering Thermophysics, Chinese Academy of Sciences
P. O. Box 2706, Beijing 100080, CHINA
Phone: +86-10-62581786, Fax: +86-10-62575913, E-mail: jjl@mail.etp.ac.cn

ABSTRACT

This paper describes the numerical simulation of 3D flows in turbine blade rows and turbine exhaust systems. The 3D Navier-Stokes flow solver used for the simulation is based upon the finite-volume TVD Lax-Wendroff scheme. The Baldwin-Lomax turbulence model is used to estimate the eddy viscosity and the V-type multigrid algorithm is used to speed up the convergence to a steady state. A simple multiblock strategy is adopted to deal with the complicated domain of exhaust systems. Numerical actuator disk model is used to simulate the presence of whole annulus blade rows in non-axisymmetric flows. The solution procedure is described and the application of the present method to a single-stage turbine and a turbine exhaust is presented.

INTRODUCTION

The main flow path of turbomachinery consists of blade rows and inlet/exhaust systems adjacent to the blade row. The steady flow solver with mixing plane approach (Denton, 1992) can be used for the analysis of flow matching between blade rows and for the prediction of blade row aerodynamic performance (Dawes, 1992). By including the deterministic stress source terms, the steady flow solver is capable of realistic prediction of multiple blade row performance (Rhie, 1998). The flow in turbine exhaust systems is strongly influenced by inflow conditions (Liu, et.al., 2003) associated with the operation of upstream turbine. Most of steam turbines and many of industrial gas turbines discharge towards one-side of the exhaust. The non-axisymmetric structure of one-side discharge results in non-axisymmetric flow fields at the turbine exit plane and in these circumstances the periodic condition for turbine blade rows is only satisfied after a whole annulus. To allow for the flow coupling between the turbine and exhaust in non-axisymmetric flows, the existence of the blade rows in the whole annulus has to be simulated properly.

This paper presents the development and application of a TVD flow solver capable of simulating 3D viscous flows in blade rows and exhaust systems. It is generally recognized that a TVD scheme incorporated with Roe's approximate

Riemann solver resolves both shear layer and flow discontinuity very well. Numerical experiment showed that the application of the TVD scheme is essential for the present flow solver to resolve the flow details with a relatively coarse mesh. Numerical actuator disk model is incorporated into the flow solver to simulate the whole annulus blade rows. Compared with simulating the 3D flows in multiple passage of a blade row around the whole annulus, the actuator disk model is effective in representing the turning and loss of the flow across the blade row in non-axisymmetric flow fields.

After this introduction, the numerical approach is described. The numerical results for a single-stage turbine and a steam turbine exhaust is then presented and discussed. The paper ends with conclusions.

NUMERICAL APPROACH

Solution Method

The Reynolds averaged Navier-Stokes equations to be solved can be written in the following non-dimensional form,

$$\frac{\partial U}{\partial t} + \frac{\partial F}{\partial x} + \frac{\partial G}{\partial y} + \frac{\partial H}{\partial z} = \frac{1}{\text{Re}_\infty} \left(\frac{\partial F_v}{\partial x} + \frac{\partial G_v}{\partial y} + \frac{\partial H_v}{\partial z} \right) + Q \quad (1)$$

Where U is the vector of conservation variables, F, G, H are the vectors of convection fluxes, F_v, G_v, H_v are the vectors of diffusion fluxes, Q is the vector of source terms. Re_∞ is Reynolds number based on the free stream state and characteristic length. Equation (1) is solved numerically by using the explicit TVD Lax-Wendroff scheme incorporated with Roe's approximate Riemann solver (Roe, 1981). The V-cycle multigrid method (Ni, 1989) is adopted to speed up the convergence to a steady state. The explicit scheme applied can be written in the following form,

$$U^{n+1} = U^n + \delta U, \quad \delta U = \delta U_h + \sum_{m=1}^N T_{2mh}^h \delta U_{2mh} \quad (2)$$

Where δU is the correction on the fine mesh, δU_{2mh} is the correction on the successive coarse meshes, T is the interpolation operator from the coarse mesh to fine mesh. When δU approaches to zero, U^{n+1} approaches to U^n and a steady solution is obtained.

The turbulent eddy viscosity is estimated by using the Baldwin-Lomax model. In this model a turbulence boundary layer is divided into an inner and an outer region. In the inner

region, the eddy viscosity is determined by

$$(\mu_t)_{inner} = \rho l^2 |\omega| \quad (3)$$

Where ρ is the fluid density, l is a length scale proportional to the distance from the wall (scaled by a damping factor D), and ω is the vorticity. In the outer region, the eddy viscosity is given by

$$(\mu_t)_{outer} = C_{outer} \rho F_{wake}^F F_{kleb} \quad (4)$$

Where C_{outer} is a constant, F_{kleb} is the intermittency factor, F_{wake} is a function of d_{max} , F_{max} , and V_{dif} (difference between maximum and minimum velocity in the profile). F_{max} is the maximum value of the function $F = d |\omega| D$, and d_{max} is the distance d (from the wall or wake center) at which this maximum occurs. For a complicated flow field, F may exhibit multiple local maximal. The maximum closest to the wall is chosen in the present implementation. Standard coefficients due to Baldwin and Lomax (1978) are used.

In practice, both inner-layer viscosity and outer-layer viscosity are computed for the entire boundary layer and the smaller one is taken as the actual eddy viscosity.

For a complicated flow domain, two solid walls (e.g., A and B) may intersect. The eddy viscosity in these circumstances is first computed according to each of the two walls and then weighted by the distance from the wall to form the effective eddy viscosity,

$$\mu_t = \frac{d_B^2 (\mu_t)_A + d_A^2 (\mu_t)_B}{d_A^2 + d_B^2} \quad (5)$$

Where d_A is the distance from wall A, d_B from the wall B.

Multiblock approach is incorporated to allow for the flow solver to deal with the complex physical domain of turbine exhausts. The mesh at a block interface is of one-to-one abutment.

Numerical Boundary Conditions

Five types of numerical boundaries may exist in the computational domain, namely, inlet, outlet, solid wall, block interface and blade row interface. Distributions of total pressure, total temperature, and tangential and radial flow angle are specified at domain inlet. Averaged static pressure is specified at domain outlet. Flow is assumed adiabatic at solid wall. To avoid using extremely fine mesh near the solid wall, the wall-function due to Spalding is applied. Block interface is an internal boundary within the computational domain. Due to nodal storage of flow variables and one-to-one abutment of the mesh at block interfaces, flows of two adjacent blocks can be connected by averaging the conservation variables at each side of the interface. Numerical experiments showed that the above treatment gives smooth transit through the interface without using an overlapped mesh. The implementation details of the numerical boundary conditions for inlet, outlet, solid wall and block interface can be found in Liu (1998).

A blade row interface separates the rotor blade row in the rotating frame and the stator blade row in the stationary frame. The one-dimensional non-reflection boundary conditions at the blade row interface are implemented in the absolute frame of reference. To do so, the Cartesian velocity components u , v , and w at a blade row interface are first converted to the cylindrical components v_x , v_θ and v_r in the

absolute frame of reference. Area-average in the circumferential direction on ρ , ρv_x , ρv_θ , ρv_r and h (total enthalpy) is then carried out at each radial location to obtain the area-averaged $\bar{\rho}$, \bar{v}_x , \bar{v}_θ , \bar{v}_r and \bar{p} . We define

$$A = \begin{pmatrix} -\bar{c}^2 & 0 & 0 & 0 & 1 \\ 0 & 0 & \bar{\rho} \cdot \bar{c} & 0 & 0 \\ 0 & 0 & 0 & \bar{\rho} \cdot \bar{c} & 0 \\ 0 & \bar{\rho} \cdot \bar{c} & 0 & 0 & 1 \\ 0 & -\bar{\rho} \cdot \bar{c} & 0 & 0 & 1 \end{pmatrix} \quad (6)$$

$$A^{-1} = \begin{pmatrix} -\frac{1}{\bar{c}^2} & 0 & 0 & \frac{1}{2\bar{c}^2} & \frac{1}{2\bar{c}^2} \\ 0 & 0 & 0 & \frac{1}{2\bar{\rho} \cdot \bar{c}} & -\frac{1}{2\bar{\rho} \cdot \bar{c}} \\ 0 & \frac{1}{\bar{\rho} \cdot \bar{c}} & 0 & 0 & 0 \\ 0 & 0 & \frac{1}{\bar{\rho} \cdot \bar{c}} & 0 & 0 \\ 0 & 0 & 0 & 0.5 & 0.5 \end{pmatrix} \quad (7)$$

Where $\bar{c} = \sqrt{\gamma \bar{p} / \bar{\rho}}$, γ is the specific heat ratio. The averaged characteristic variables at the interface are calculated by

$$[\bar{\alpha}_1, \bar{\alpha}_2, \bar{\alpha}_3, \bar{\alpha}_4, \bar{\alpha}_5]^T = A [\bar{\rho}, \bar{v}_x, \bar{v}_\theta, \bar{v}_r, \bar{p}]^T \quad (8)$$

The predicted local characteristic variables at the interface are calculated by

$$[\alpha_1, \alpha_2, \alpha_3, \alpha_4, \alpha_5]^T_p = A [\rho, v_x, v_\theta, v_r, p]^T_p \quad (9)$$

The new local flow variables at the interface are obtained by

$$[\rho, v_x, v_\theta, v_r, p]^T_{new} = A^{-1} [\alpha_1, \alpha_2, \alpha_3, \alpha_4, \alpha_5]^T_{new} \quad (10)$$

For the upstream boundary of the interface, i.e., the outlet of the upstream blade row, if the local axial speed is subsonic, for example, we set

$$[\alpha_1, \alpha_2, \alpha_3, \alpha_4, \alpha_5]^T_{new} = [\alpha_1^p, \alpha_2^p, \alpha_3^p, \alpha_4^p, \bar{\alpha}_5]^T \quad (11)$$

Likewise for the downstream boundary of the interface, i.e., the inlet the downstream blade row, we set

$$[\alpha_1, \alpha_2, \alpha_3, \alpha_4, \alpha_5]^T_{new} = [\bar{\alpha}_1, \bar{\alpha}_2, \bar{\alpha}_3, \bar{\alpha}_4, \alpha_5^p]^T \quad (12)$$

The obtained new local flow variables in the absolute frame of reference are then converted back to the local frame of reference and to the Cartesian coordinate system. The conversation variables are finally modified by using the new flow variables. The present implementation of the blade row interface boundary conditions allows for reverse local flow across the interface.

Actuator Disk Model

The actuator disk model is used to represent the whole annulus blade row in non-axisymmetric flows. Flow variables across the disk can jump in order to achieve the flow turning and entropy rise occurred within the blade row. Numerically speaking, an actuator disk is a boundary that is geometrically continuous and physically discontinuous. The two flow fields separated by the disk can be calculated

respectively by the 3D flow solver and connected by disk boundary conditions. The disk boundary conditions should preserve the conservation of mass flow, momentum and energy. It is assumed in the present actuator disk model that the streamlines across the actuator disk are continuous and the slope of a streamline is also continuous at the two sides of the disk. Five disk boundary conditions are then derived. The details of the disc boundary conditions can be found in Liu and Hynes (2003).

RESULTS AND DISCUSSIONS

Single-Stage Turbine

The geometry of stator and rotor blade and the experimental data were reported in Moffit et.al. (1980). The 3D mesh used for the simulation is shown in Fig.1. The mesh dimensions are $89 \times 21 \times 21$ for the stator and also for the rotor. The inlet and outlet boundary conditions are the same with the experiments. Averaged static pressure is specified at the hub end wall at the rotor outlet and pressure at other radial locations is determined by using the equation of radial equilibrium and the local flow.

The computed and measured isentropic Mach number distributions at the tip, mid span and hub of the stator blade are shown in Fig.2. The agreement between the computed results and the experimental data is good at hub and mid span. There were discrepancies at the suction surface at the blade tip. These discrepancies were also noticed in the calculations using different flow solvers by previous researchers. The reason for the discrepancy between numerical results and experimental data at the tip of the stator requires further investigation.

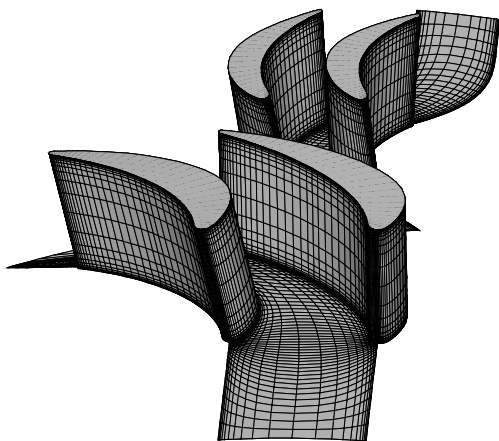
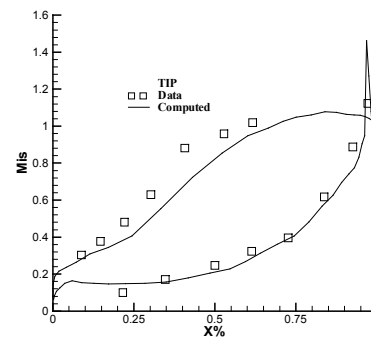
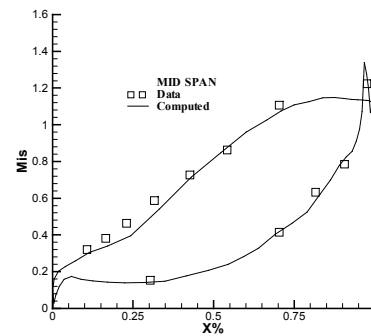


Fig.1 3D Mesh used for the single-stage turbine

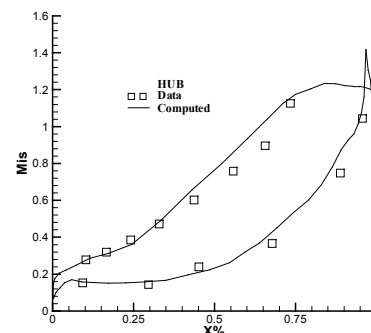
The computed Mach contours at mid span of the single stage turbine are shown in Fig.3. The computed stream traces at the mid span of rotor blade are shown in Fig.4. A small separation bubble at the pressure surface of the rotor blade is noticed, which indicates that the profile of rotor blade at mid span may need to be modified. The computed pressure distributions at the stator and rotor blade surface at mid span are shown in Fig. 5. The flow expansion (i.e., pressure decrease) in the stator and then in the rotor is seen. By using the non-reflection boundary conditions at the stator and rotor interface, the pressure jump at the interface is very small.



(a) Stator tip



(b) Stator mid span



(c) Stator hub

Fig.2 Isentropic Mach number distributions: (a) stator tip, (b) stator mid span, (c) stator hub

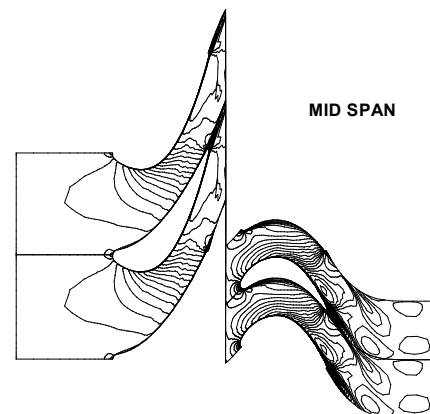


Fig.3 Computed Mach number contours at mid span of the single stage turbine

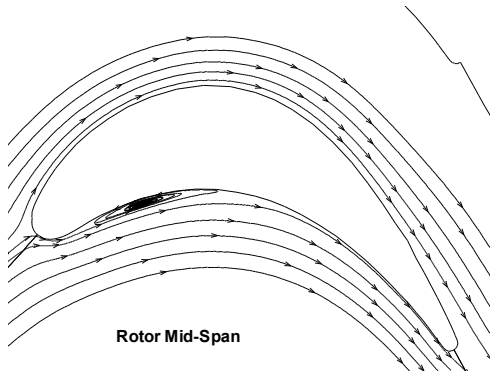


Fig.4 Computed stream traces at mid span of the rotor blade

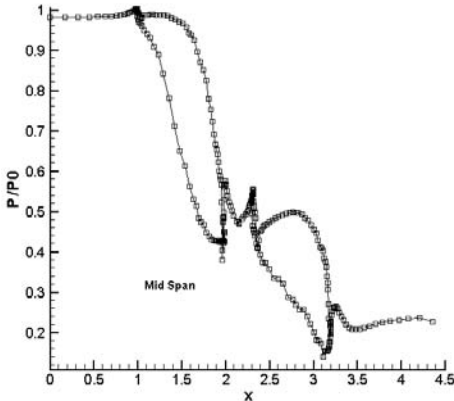


Fig.5 Computed static pressure distributions at mid span of the single stage turbine

Steam Turbine Exhaust

The 3D hexahedral mesh used for the turbine-exhaust interactions is shown in Fig.6. The mesh consists of the flow domains of stator, rotor, diffuser and collector. The mesh dimensions are $9 \times 65 \times 25$ for the stator and also for the rotor, $49 \times 65 \times 25$ for the diffuser and $89 \times 113 \times 25$ for the collector, respectively. About 360,000 nodes are applied for the simulation. The locations of the stator and rotor blade row are illustrated in Fig.7. Two actuator disks are placed at the trailing edges of the stator and rotor blade to simulate the whole annulus blade rows in non-axisymmetric flows.

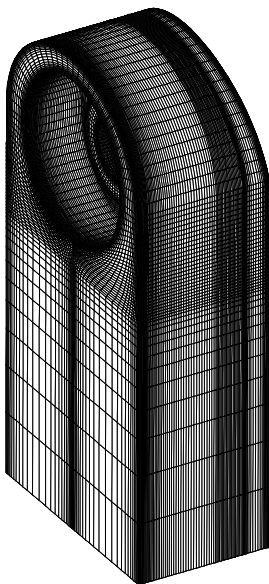


Fig.6 3D mesh used for the turbine-exhaust interactions

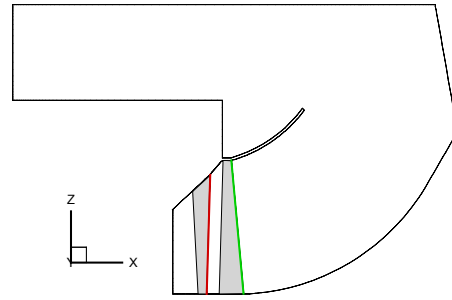


Fig.7 Illustration of the stator and rotor blade row, actuator disks are placed at the blade trailing edges

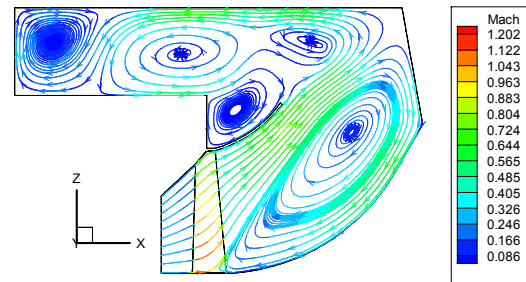


Fig.8 Stream traces at $\theta = 0$ deg

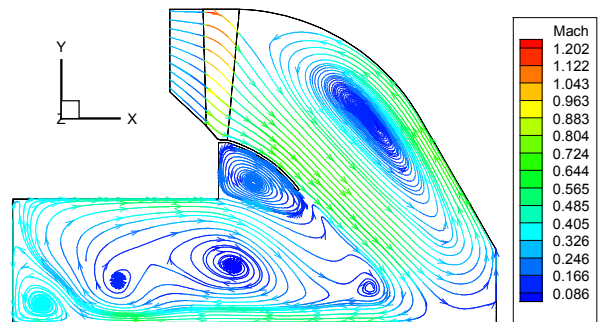


Fig.9 Stream traces at $\theta = -90$ deg

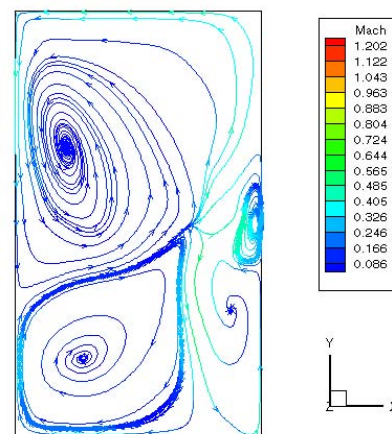


Fig.10 Stream traces at exhaust exit

Stream traces are streamlines plotted in a 2D section of the 3D flow domain. A stream trace usually starts at the domain inlet and ends at vortex center or other domain boundary (e.g., domain outlet). Stream traces at several typical

sections around the annulus of the exhaust hood are plotted.

Figure 8 shows the stream traces at the top of the exhaust ($\theta = \arctan(y/z) = 0$ deg). It can be seen that a large vortex occupies the inner part of the diffuser, which significantly reduces the diffuser effective area and therefore reduces the capability of pressure recovery. Two pairs of vortices are also noticed in the collector.

The section of $\theta = -90$ deg corresponds to the one side of the exhaust horizontal flange. The stream traces at this section are shown in Fig.9. The large vortex noticed at the section of $\theta = 0$ deg still appears in the flow domain of diffuser. The structures of the vortices in the collector at this section are complicated.

Figure 10 shows the stream traces at the exhaust exit. Two large passage vortices are noticed in the left-hand side, which are developed from the vortices in the upstream collector. Two small vortices are noticed in the right-hand side, which are developed from the vortices in the diffuser.

CONCLUSIONS

The 3D multiblock Navier-Stokes solver based upon the TVD Lax-Wendroff scheme and the application of the solver to the simulation of 3D flows in the single-stage turbine and the turbine exhaust have been presented. The solver well predicted the blade surface isentropic Mach number distributions of the single-stage turbine. It also predicted the possible separation near the rotor pressure surface at the mid span. By incorporating with the numerical actuator disk model, the solver is capable of predicting the complex coupling flow between the turbine and exhaust system in asymmetric flows.

ACKNOWLEDGEMENTS

The author gratefully acknowledges the financial support provided by the National 973 Program of China and Knowledge Innovation Program of Chinese Academy of Sciences.

REFERENCES

- Baldwin, B.S., and Lomax, H., 1978 "Thin Layer Approximation and Algebraic Model for Separated Turbulent Flows", AIAA Paper No.78-257
- Dawes, W.N., 1992, "Towards Improved Throughflow Capability: The Use of 3D Viscous Flow Solvers in a Multistage Environment", *ASME Journal of Turbomachinery*, Vol.114
- Denton, J.D., 1992, "The Calculation of Three-Dimensional Viscous Flow Through Multistage Turbomachinery", *ASME Journal of Turbomachinery*, Vol.114
- Liu, J.J., 1998, "The Calculation of Asymmetric Flow in Turbine Exhaust Systems", PhD Thesis, Cambridge University Engineering Department, United Kingdom.
- Liu, J.J., Cui, Y.Q. and Jiang, H.D., 2003, "Investigation of Flow in a Steam Turbine Exhaust Hood With/Without Turbine Exit Conditions Simulated", *ASME Journal of Engineering for Gas Turbines and Power*, Vol.125, pp292-299
- Liu, J.J., and Hynes, T.P. 2003, "The Investigation of Turbine and Exhaust Interactions in Asymmetric Flows — Blade Row Models Applied", *AMSE Journal of Turbomachinery*, Vol.125, pp121-127
- Moffit, T.P., Szanca, E.M., and Whitney, W.J., 1980, "Design and Cold Air Test of Single Stage Uncooled Core Turbine With High Work Output", NASA TP-1680
- Ni, R.H., 1989, "Prediction of 3D Multi-Stage Turbine Flow

Field Using a Multiple-Grid Euler Solver", AIAA paper No.89-0203.

Rhie, C.M., etal, 1998, "Development and Application of a Multistage Navier-Stokes Solver, Part I & II", *ASME Journal of Turbomachinery*, Vol.120

Roe, P.L., 1981, "Approximate Riemann Solvers, Parameter Vectors and Difference Schemes", *Journal of Computational Physics*, Vol.43, pp.357-372h